Dalton Transactions

ROYAL SOCIETY OF CHEMISTRY

PAPER

View Article Online
View Journal | View Issue

Cite this: *Dalton Trans.*, 2026, **55**, 7612

Steric tuning of OH-functionalised *N*,*N*-manganese(I) complexes for the transfer hydrogenation of carbonyl compounds

Samuel J. Prettyman, [a] Saad Alqahtani,[b] Mona H. Alhalafi,[a,c] Kuldip Singh[a] and Gregory A. Solan *[a]

A new family of manganese(I) carbonyl complexes, [2-OH-6-{CMe=N(2,6-R^1_2-4-$R^2C_6H_2$)}C_5H_3N]MnBr$(CO)_3$ (R^1 = ^{i}Pr, R^2 = H **Mn1a**, R^1 = ^{i}Pr, R^2 = Br **Mn1b**, R^1 = H, R^2 = ^{i}Pr **Mn1d**, R^1 = H, R^2 = Me **Mn1e**), bearing 6-(arylimino)pyridine N,N-chelating ligands that are appended with a 2-hydroxyl group, have been synthesised and evaluated as catalysts in the transfer hydrogenation (TH) of acetophenone and its derivatives. This set of complexes, differing in their steric and electronic properties of their *N*-aryl groups, reveal distinct catalytic performances with the least sterically hindered *N*-4-isopropylphenyl derivative, **Mn1d**, the most active allowing TON's of up to 1030. Moreover, **Mn1d** proved highly effective for an assortment of aryl-methyl ketones with the steric/electronic profile of the substrate having an observable effect on conversion. Mechanistic studies involving DFT calculations point towards an outer-sphere mechanism that is distinctly affected by the steric properties of the *N*-aryl groups of the manganese catalyst.

Received 25th March 2026,
Accepted 22nd April 2026

DOI: 10.1039/d6dt00709k

rsc.li/dalton

Introduction

Within the field of transition metal (TM) catalysis, there is an on-going drive to develop more sustainable alternatives to precious metal systems that have long formed the cornerstone of homogeneous catalysis.[1,2] Notably, base metal catalysts drawn from the first row of the TMs have seen the emergence of molecular systems that are starting to approach the levels of performance displayed by their precious metal counterparts. One such area that has attracted attention in recent years is the use of manganese(I) complexes as these have shown promise as catalysts for a number of organic transformations.[3,4]

With a view to improving the efficacy of such low valent Mn catalysis, the installation of non-innocent or functionalised ligands has been increasingly developed to access lower energy transition states in catalytic transformations or to imbue the complex with desirable properties.[1,5–10] In terms of the functionalised ligand itself, this can assist the metal centre through the use of pendant groups to help direct substrates or to act as a redox active unit. These redox active ligands work in concert with the metal centre to promote reversible transformations during the catalysis such as protonation/deprotonation of the ligand so as to accelerate catalysis.[8]

While much progress has been reported with NH-functionalised P,N,P and P,N,N ligands on manganese,[9] research directed towards smaller and simpler bidentate systems incorporating a range of potentially redox non-innocent donor units including imines, has only recently started to emerge.[10] Of note, a number of pyridine-containing examples functionalised with OH groups have displayed great potential (Fig. 1),[11–20] whereby the synergistic pairing of the hydroxy functionality and a manganese(I) centre has seen catalysts

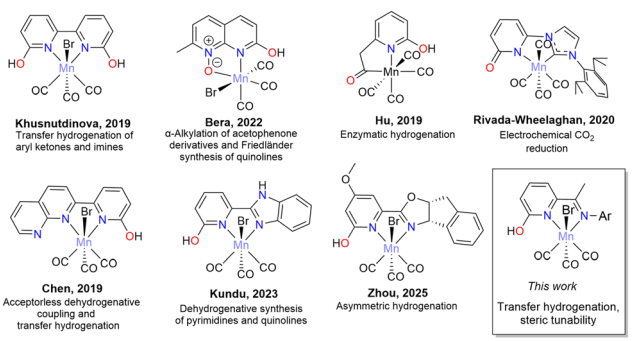

Fig. 1 Previously reported manganese(I) complexes incorporating hydroxyl-functionalised pyridine-based chelating ligands, along with the target of this work.

[a]*School of Chemistry, University of Leicester, University Road, Leicester, LE1 7RH, UK. E-mail: gas8@leicester.ac.uk; Tel: +44-1162522096*
[b]*Department of Chemistry, College of Science, King Saud University, Riyadh 11451, Saudi Arabia*
[c]*Department of Chemistry, College of Science, Majmaah University, 11952, Saudi Arabia*

capable of facilitating a wide range of transformations under increasingly mild conditions.

In the context of transfer hydrogenation (TH), manganese(I) catalysis has witnessed some marked improvements[9,13,17–26] with TONs of up to 17 300 reported.[10d,g] Notwithstanding these developments the mechanistic details of the reaction pathways followed remain uncertain with both inner- and outer-sphere mechanisms postulated.[4,9,27–33] Furthermore, the impact of steric effects and, to a lesser degree, electronic factors of the catalyst on the mechanistic pathway remains relatively unexplored.[34]

Herein we report the synthesis of a novel series of manganese(I) carbonyl bearing 2-hydroxy-6-(arylimino)pyridine ligands differing in the steric and electronic profile of the *N*-aryl groups (Fig. 1). These complexes are then investigated as catalysts for the TH of firstly acetophenone and then a series of derivatives to explore the role of these steric/electronic variations on catalyst performance. To complement the experimental work, DFT calculations are performed to probe the mechanistic pathway and the role played by these steric effects.

Results and discussion

Synthesis of 6-arylimino-2-pyridone

The 6-arylimino-2-pyridones, 6-{CMe=N(2,6-R^1_2-4-$R^2C_6H_2$)}C_5H_3NH-2-O (R^1 = ^{i}Pr, R^2 = H **HL1a**, R^1 = ^{i}Pr, R^2 = Br **HL1b**, R^1 = R^2 = ^{i}Pr **HL1c**, R^1 = H, R^2 = ^{i}Pr **HL1d**, R^1 = H, R^2 = Me **HL1e**), were synthesised in moderate to good yield *via* the condensation reaction of 6-acetyl-pyrid-2-one with the corresponding *ortho*- and *para*-substituted anilines in *n*-butanol at elevated temperature in the presence of an acid catalyst (Scheme 1). The 6-acetyl-pyrid-2-one starting material is not commercially available but could be readily obtained in two steps from 2-bromo-6-methoxypyridine. Confirmation that **HL1a**–**HL1e** adopt the 2-pyridone tautomer over the 2-pyridinol one was provided by single crystal X-ray diffraction studies performed on **HL1a** and **HL1e** (see SI). Indeed, free 6-substituted 2-pyridones generally have a tendency to adopt this tautomer.[35,36] Some variation in the solubility of **HL1a**–**HL1e** was seen with **HL1a**–**HL1c** displaying good solubility in hexane likely due to the increase in solubilising isopropyl groups on the *N*-aryl ring, whilst **HL1d** and **HL1e** proved noticeably less soluble.

Syntheses of Mn1a–Mn1e and Mn2

The orange crystalline complexes, [2-OH-6-{CMe=N(2,6-R^1_2-4-$R^2C_6H_2$)}C_5H_3N]MnBr(CO)$_3$ (R^1 = ^{i}Pr, R^2 = H **Mn1a**, R^1 = ^{i}Pr, R^2 = Br **Mn1b**, R^1 = H, R^2 = ^{i}Pr **Mn1d**, R^1 = Me, R^2 = Me **Mn1e**) were typically prepared in good yield by reacting **HL1a**, **HL1b**, **HL1d** and **HL1e** with a stoichiometric amount of manganese pentacarbonyl bromide in dichloromethane or diethyl ether overnight at 30 °C (Scheme 2). Conversely, [2-OH-6-{CMe=N(2,4,6-^{i}Pr$_3C_6H_2$)}C_5H_3N]MnBr(CO)$_3$ (**Mn1c**), owing to the greater solubility of **HL1c**, was prepared using hexane at reflux to afford **Mn1c** as a bright orange powder.

Single crystals of **Mn1a**–**Mn1e** suitable for X-ray diffraction studies were grown from methanol upon standing for 48 hours at room temperature. A view of representative **Mn1d** is shown in Fig. 2, while selected bond distances and angles are given in the caption (see SI for **Mn1a**, **Mn1b**, **Mn1c** and **Mn1e**). The structures of **Mn1a**–**Mn1e** are isostructural and based on a distorted octahedral arrangement in which the bromide and the two N-donor atoms of the chelating N,N-ligand are *trans* to carbonyl groups, while the third CO is *trans* to a bromide. In

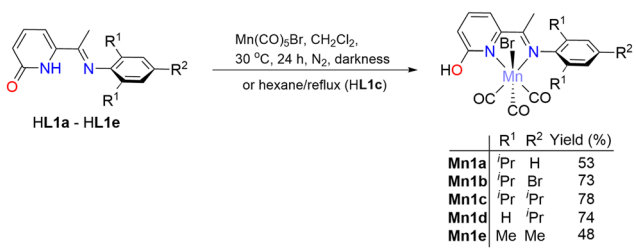

	R^1	R^2	Yield (%)
Mn1a	^{i}Pr	H	53
Mn1b	^{i}Pr	Br	73
Mn1c	^{i}Pr	^{i}Pr	78
Mn1d	H	^{i}Pr	74
Mn1e	Me	Me	48

Scheme 2 Preparation of **Mn1a**–**Mn1e** from **HL1a**–**HL1e**.

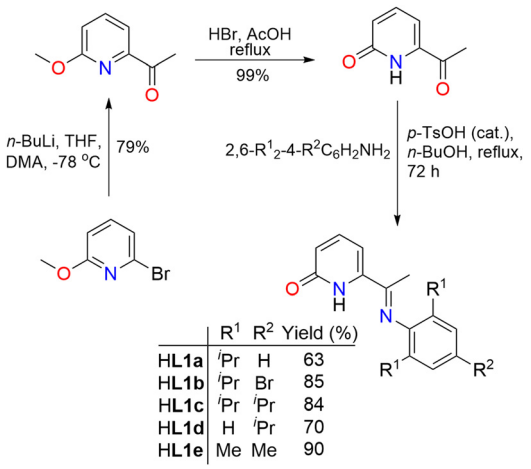

	R^1	R^2	Yield (%)
HL1a	^{i}Pr	H	63
HL1b	^{i}Pr	Br	85
HL1c	^{i}Pr	^{i}Pr	84
HL1d	H	^{i}Pr	70
HL1e	Me	Me	90

Scheme 1 Synthetic route to the 6-arylimino-2-pyridones, **HL1a**–**HL1e**.

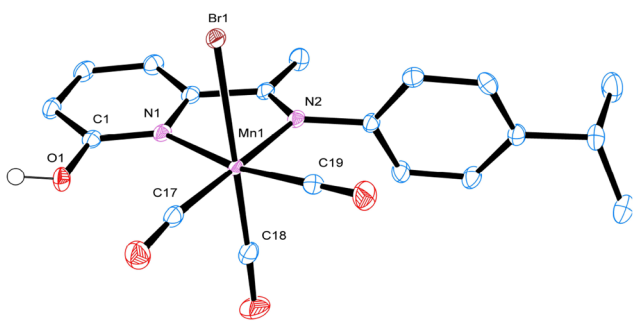

Fig. 2 ORTEP representation of **Mn1d** with the thermal elipsoids set to 50% probability. All protons except for H(1) have been removed for clarity. Selected bond distances (Å): Br(1)–Mn(1) 2.5470(3), Mn(1)–N(1) 2.0736(14), Mn(1)–N(2), 2.0300(14). Selected bond angles (°): N(1)–Mn(1)–Br(1) 84.57(4), N(2)–Mn(1)–N(1) 77.69(5), C(18)–Mn(1)–Br(1), 179.64(6). Selected torsion angle (°): N(2)–C(8)–C(9)–C(10) 178.70(15).

terms of the N,N-ligand, this now adopts the 2-pyridinol form following coordination to the Mn(I) centre. Interestingly, the bulkier 2,6-substituted *N*-aryl groups in **Mn1a**, **Mn1b** and **Mn1c** impart some distortion along the Br(1)–Mn(1)–CO axis with corresponding angles of 169.76(8)°, 170.53(7)° and 171.40 (12)°, respectively. By contrast in **Mn1d** the corresponding Br–Mn–CO bond angle was found to be 179.64(6)° highlighting the minimal effect of the *N*-4-^{i}PrC$_6$H$_5$ group on this axis. Furthermore, the Mn(1)–N(2)$_{imine}$ bond distance provides a valuable indicator on the steric properties imparted by the *N*-aryl *ortho* substituents with this bond length increasing in the order: **Mn1a** (2,6-^{i}Pr$_2$) > **Mn1e** (2,6-Me$_2$) > **Mn1d** (2,6-H$_2$). In all cases, the O(1)–H proton is involved in intermolecular hydrogen bonding leading to some form of multimetallic assembly. For **Mn1a**, **Mn1b**, **Mn1c** and **Mn1e**, lattice methanol is additionally incorporated into the assembly, while **Mn1d** makes use of solely O(1)H···Br interactions.

The IR data for **Mn1a–Mn1e** reveal three strong carbonyl absorption bands with modest variation between complexes. For the 2,6-diisopropyl-containing **Mn1a**, **Mn1b** and **Mn1c**, the average carbonyl stretching frequency is the highest for *para*-bromo **Mn1b** (1958 cm^{-1} *vs.* 1953 cm^{-1} for **Mn1a** and **Mn1c**) which is in line with the least back-donation into the CO ligands on account of the electron withdrawing bromide. This trend is also reflected in the ^{13}C NMR spectra in which the average of the chemical shifts for the three carbonyl resonances for **Mn1b** is the most downfield for this series of complexes. In the ^{1}H NMR spectra, the OH protons can be seen in a narrow downfield range between δ 12.45–13.31 in keeping with their involvement in hydrogen bonding as seen in the X-ray structures.

For comparative purposes the related *N*,*O*-manganese complex, [2-OH-6-(CMe=O)C$_5$H$_3$N]MnBr(CO)$_3$ (**Mn2**), was also synthesised from 6-acetyl-pyrid-2-one and structurally characterised (Fig. 3).[37] As expected, the introduction of the N,O-ligand has a notable effect on the carbonyl resonances in the ^{13}C NMR spectrum with a downfield shift clearly evident from that seen for **Mn1a–Mn1e** suggesting a sizable difference in back-bonding, which is also reflected by a dramatic increase in the average carbonyl bond stretching frequency (Table 1).

Derivatisation and solvent dependent deprotonation

During attempts at growing crystals of the manganese complexes for X-ray diffraction, it became evident that the type of crystallising solvent and the time spent in the solvent could lead to aggregation, following deprotonation and partial oxidation of the metal centre. For example, attempted crystallisation of **Mn1d** from a dimethylformamide (DMF) solution layered with diethyl ether gave after several weeks red blocks of the trinuclear species, [[2-*O*-6-{CMe=N(4-^{i}PrC$_6$H$_4$)}C$_5$H$_3$N]MnBr(CO)$_3$]$_2$Mn(DMF)$_4$ (**Mn1d′**) in which a Mn(II)(DMF)$_4$ fragment in sandwiched between two (*N*,*N*)Mn(I) units (Fig. 4). Evidently, the deprotonation of the 2-pyridinol unit is a facile process which we believe is pivotal to the function of the catalyst (see later). Curiously, partial deprotonation and scavenging of a CO was observed when **Mn1b** was crystallised from a mixture of dichloromethane and hexane forming yellow blocks of co-crystallised **Mn1b**···[2-*O*-6-{CMe=N(2,6-^{i}Pr$_2$-4-BrC$_6$H$_2$)}C$_5$H$_3$N]Mn(CO)$_4$ (**Mn1b′**) which associate through hydrogen-bonding to form a dimeric pair (Fig. 5). Interestingly, compari-

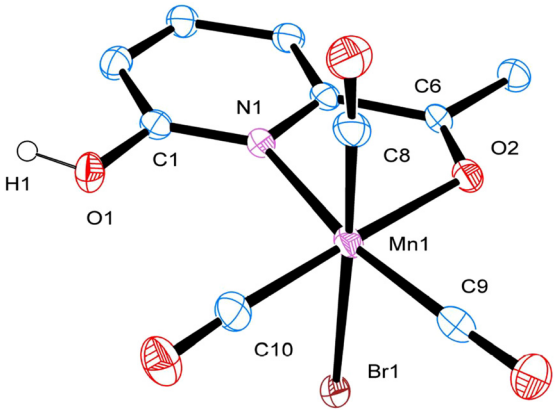

Fig. 3 ORTEP representation of **Mn2** with thermal ellipsoids set to 50% probability. All protons, apart from H1, have been removed for clarity. Selected bond distances (Å) Br(1)–Mn(1) 2.5477(9), Mn(1)–N(1) 2.091(4), Mn(1)–O(2) 2.033(4), Mn(1)–C(8) 1.805(5), Mn(1)–C(9) 1.806(6), Mn(1)–C (10) 1.808(6). Selected bond angles (°): O(2)–Mn(1)–Br(1) 87.24(10), O(2)–Mn(1)–N(1) 77.51(15), C(8)–Mn(1)–Br(1) 176.76(18), C(18)–Mn(1)–Br (1) 179.64(6).

Table 1 ^{13}C{^{1}H} NMR signals for the Mn–CO's and the CO stretching frequencies in **Mn1a–Mn1e** and **Mn2**

Complex	^{13}C NMR carbonyl signals[a] (δ, ppm)	ν(CO) stretching frequency[b] (cm^{-1})
Mn1a	220.9, 222.3, 222.9	2018, 1937, 1903
Mn1b	220.9, 222.5, 222.9	2019, 1954, 1901
Mn1c	220.4, 221.6, 222.4	2018, 1937, 1903
Mn1d	220.6, 221.8, 222.7	2024, 1940, 1904
Mn1e	221.3, 222.4, 222.6	2020, 1940, 1897
Mn2	219.3, 223.4, 225.6	2037, 1950, 1926

[a] Recorded in DMSO-d_6 at 298 K. [b] FT-IR data recorded in the solid state.

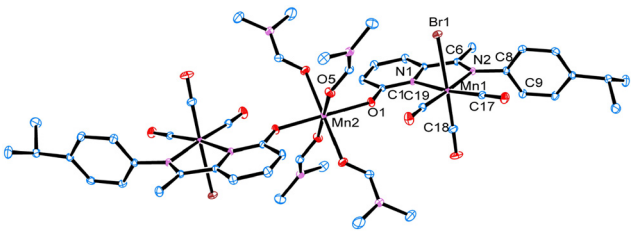

Fig. 4 ORTEP representation of **Mn1d′** with the thermal ellipsoids set to 50% probability. Grown for a 'half' asymmetric unit through symmetry operation $-x$, $-y + 1$, $-z + 1$. All protons have been removed for clarity. Selected bond distances (Å): Br(1)–Mn(1) 2.5295(4), Mn(1)–N(1) 2.0535 (16), Mn(1)–N(2), 2.0332(16), C(1)–O(1) 1.274(2), O(1)–Mn(2) 2.1485(14). Selected bond angles (°): N(1)–Mn(1)–Br(1) 86.57 (4), N(2)–Mn(1)–N(1) 77.91(6), C(18)–Mn(1)–Br(1), 178.36(11), O(5)–Mn(2)–O(6) 92.31(5).

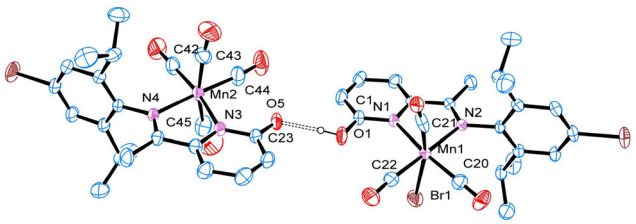

Fig. 5 ORTEP representation of **Mn1b′** with thermal ellipsoids set to 50% probability. All protons, apart from H1, have been removed for clarity. Selected bond distances (Å): Mn(1)–N(1) 2.053(4), Mn(1)–N(2) 2071(4), Mn(1)–Br(1) 2.5343(11), Mn(1)–C(20) 1.815(6), Mn(1)–C(21) 1.813 (8), Mn(1)–C(22) 1.805(6), C(1)–O(1) 1.323(7), Mn(2)–N(3) 2.081(4), Mn (2)–N(4) 2.078(4), Mn(2)–C(42) 1.805(7), Mn(2)–C(43) 1.859(8), Mn(2)–C (44) 1.799(7), Mn(2)–C(45) 1.854(9), C(23)–O(5) 1.266(7). Selected bond angles (°): N(2)–Mn(1)–N(1) 77.67(15), C(21)–Mn(1)–Br(1) 166.73(19), N(3)–Mn(2)–N(4) 76.83(17), C(45)–Mn(2)–C(43) 167.2(3).

son of the C(1)–O(1) and C(23)–O(5) bond lengths in these neighbouring molecules highlight the presence of a 2-pyridinol C–O bond (1.323(7) Å) and a 2-pyridonate C═O bond (1.266(7) Å), respectively; an observation that elegantly highlights the proton responsiveness of the OH functional group.[11]

Transfer hydrogenation catalysis

To explore the effectiveness of **Mn1a–Mn1e** and **Mn2** as catalysts for transfer hydrogenation, the conversion of acetophenone (**1a**) to 1-phenyl ethanol (**2a**) was chosen as the test transformation (Table 2).[11,17] Typically, these reactions were performed in isopropanol as the hydrogen source, potassium *tert*-butoxide as the base with the run temperature maintained at 80 °C over a 24-hour run time. An initial screen, based on a [Mn] : [KO^{t}Bu] : [acetophenone] ratio of 1 : 5 : 100, showed a range in levels of catalytic activity with **Mn1d** > **Mn1e** > **Mn1c** ~ **Mn1b** > **Mn1a** ≫ **Mn2** (entries 1–6, Table 2). Of those tested, **Mn1d** showed the highest activity (S/C = 100/1, 96% conversion, entry 4, Table 2), while 6-acetyl-2-pyridone **Mn2** was almost inactive (13% conversion, entry 6, Table 2). Within the 6-arylimino-2-pyridone series, **Mn1d** was the most active which would suggest the reduced steric properties of the *N*-4-isopropylphenyl group are highly influential. As a control, Mn(CO)$_5$Br which is known to have some catalytic ability in other transformations,[38] MnBr$_2$ as well as free H**L1d** were also tested (entries 7–9, Table 2); the conversions were however significantly lower than any of the catalysts synthesised in this work.

Subsequently, **Mn1d** was then used alone to identify an optimised set of conditions using acetophenone as the test substrate (entries 10–19, Table 2). Firstly, by systematically

Table 2 Catalytic evaluation for the TH of acetophenone and subsequent optimisation of **Mn1d**[a]

Entry	Catalyst (mol%)	Base (mol%)	Conversion (%)
1	**Mn1a** (1)	K^{t}BuO (5)	58
2	**Mn1b** (1)	K^{t}BuO (5)	65
3	**Mn1c** (1)	K^{t}BuO (5)	65
4	**Mn1d** (1)	K^{t}BuO (5)	96
5	**Mn1e** (1)	K^{t}BuO (5)	80
6	**Mn2** (1)	K^{t}BuO (5)	13
7	Mn(CO)$_5$Br (1)	K^{t}BuO (5)	8
8	MnBr$_2$ (1)	K^{t}BuO (5)	8
9	H**L1d**	K^{t}BuO (5)	5
10	**Mn1d** (0.5)	K^{t}BuO (5)	94
11	**Mn1d** (0.5)	K^{t}BuO (3)	98
12	**Mn1d** (0.5)	K^{t}BuO (1)	56
13	**Mn1d** (0.5)	K^{t}BuO (10)	72
14	**Mn1d** (0.5)	K^{t}BuO (20)	75
15	**Mn1d** (0.5)	Na^{t}BuO (3)	60
16	**Mn1d** (0.5)	KOH (3)	33
17	**Mn1d** (0.5)	NaOH (3)	56
18	**Mn1d** (0.5)	None	0
19[b]	**Mn1d** (0.03)	K^{t}BuO (0.18)	34
20[c]	**Mn1d** (0.5)	K^{t}BuO (3)	96

[a] Reaction conditions: catalyst (*x* mol%), base (*x* mol%), acetophenone (2 mmol) in ^{i}PrOH (5 mL) at 80 °C for 24 h in darkness. Spectroscopic conversions (%) were measured using quantitative ^{1}H NMR spectroscopy. [b] Reaction time 48 h. [c] Reaction time 4 h.

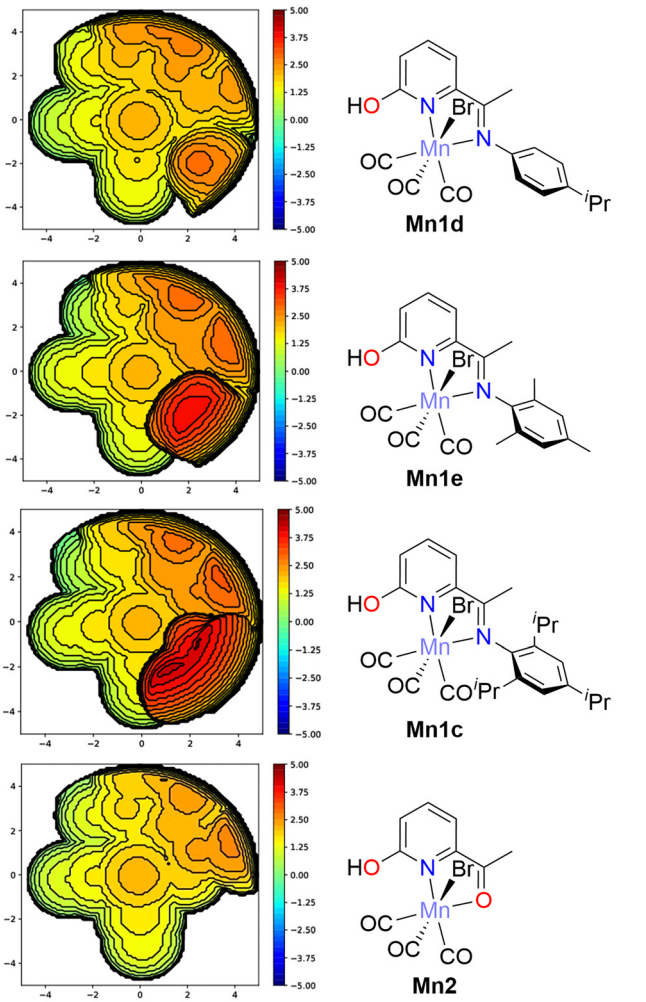

Fig. 6 SambVca generated steric maps of the (*N*,*N*)Mn(CO)$_3$ or (*N*,*O*)Mn(CO)$_3$ fragments in **Mn1c**, **Mn1d**, **Mn1e** and **Mn2** showing the buried volume (V_{bur}) around the catalytic centre.[43] Map radius set to 5 Å, bromine atom removed with positional representation of molecules orientation. For **Mn1a** and **Mn1b** see SI.

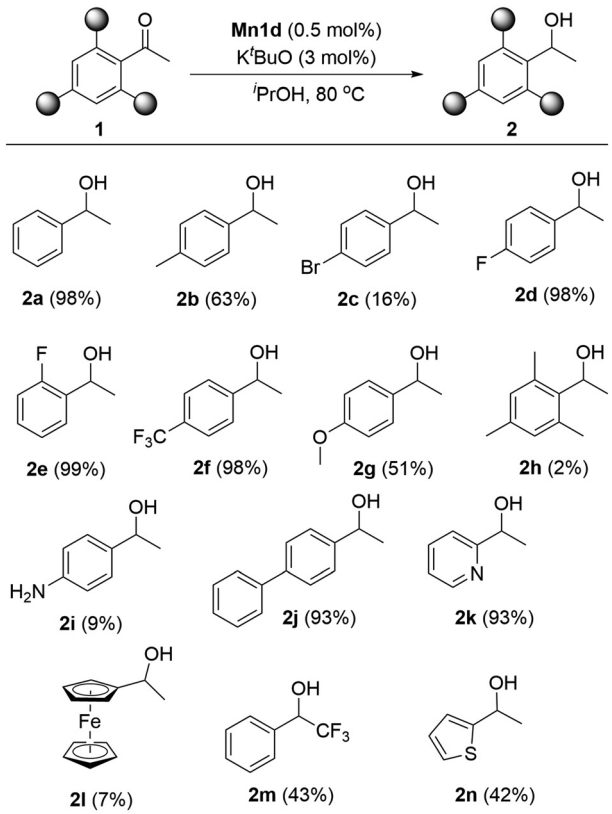

Scheme 3 TH of a selection of substituted (hetero)aryl-methyl ketones. Optimised reaction conditions as follows: catalyst (0.01 mmol), base (0.06 mmol), ketone (2 mmol) in ^{i}PrOH at 80 °C for 24 h in darkness. Spectroscopic conversions (%) were measured using quantitative ^{1}H NMR spectroscopy.

varying the [**Mn1d**] : [KOBu^t] : [**1a**] ratio, it was found that a ratio of 1 : 6 : 200 gave the highest conversion of 98% (entry 11, Table 2). Secondly, the type of base was screened by additionally employing Na^{t}BuO, KOH and NaOH with the result that KOBu^t remained the most effective (entries 11 and 15–17, Table 2); an observation that has some literature precedent.[11,17,39–42] As a control experiment, the absence of base gave 0% conversion (entry 18, Table 2). Notably with the substrate to catalyst ratio (S/C) increased to 3000/1, a 34% conversion could still be attained, which corresponds to a TON of 1030 (entry 19, Table 2).

Given that the initial TH testing had all been conducted over 24 hours, it was decided to probe the catalytic performance of these manganese catalysts over shorter run times.[11,40] Hence, by monitoring the reaction progress of **Mn1d** under optimised conditions at regular intervals it became clear that there was a rapid conversion of 81% after just 0.5 h. This then increased to 96% after 4 h before reaching a plateau (entry 20, Table 2). It is possible that the diffusion of the catalyst and substrate within the solution could justify the slower second stage of the reaction.

To probe the steric effects observed in the catalysis, the percentage buried volume (V_{bur}) around the potential active catalytic site was computed for **Mn1c**, **Mn1d**, **Mn1e** and **Mn2** (Fig. 6). It can be noted that in the southeastern (SE) quadrant in the figure, a trend in decreasing free volume is seen: **Mn1d** (40%) > **Mn1e** (29.4%) > **Mn1c** (23.9%). This decrease in free volume between **Mn1c** and **Mn1d** suggests reduced access to the active site supporting the experimentally determined conversions. As expected, ketone-containing **Mn2** exhibits an even greater value for V_{bur} in the SE quadrant (69.4%).

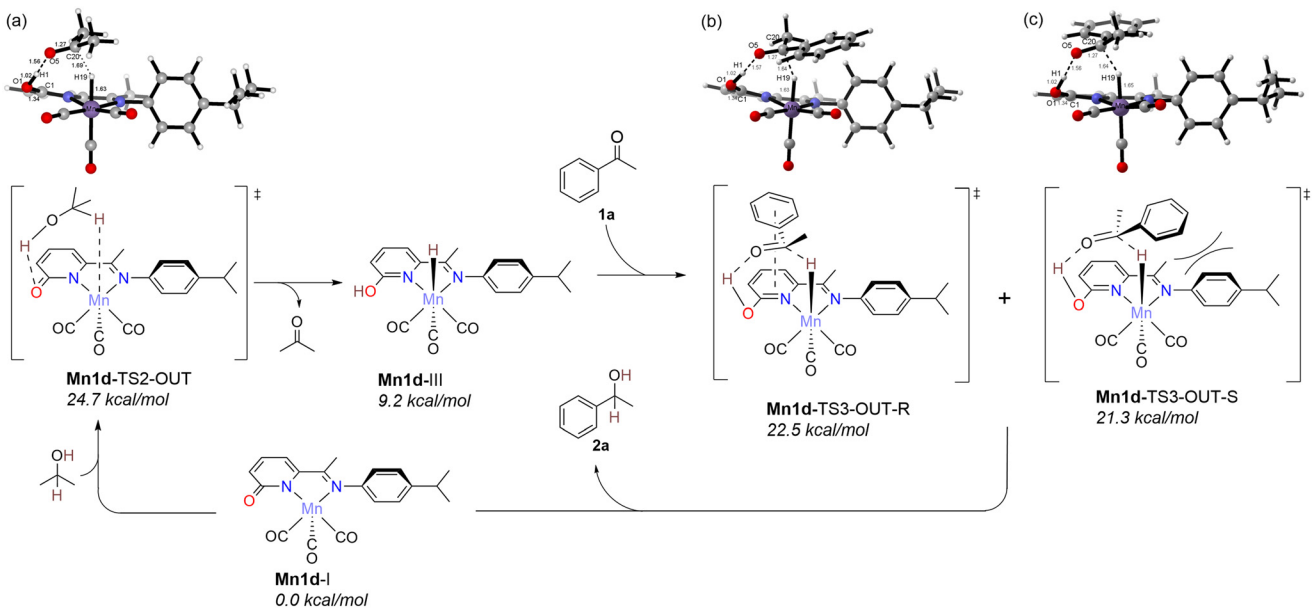

Scheme 4 DFT calculated energy pathway for the proposed outer sphere mechanism for the transfer hydrogenation of **1a** using **Mn1d** in isopropanol with geometry-optimised coordinates of transition states (a) **Mn1d**-TS2-OUT, (b) **Mn1d**-TS3-OUT-R and (c) **Mn1d**-TS3-OUT-S shown above. The solvent corrected energy values are shown in italics, while associated bond distances/interactions in the (a), (b) and (c) are in Å.

With **Mn1d** identified as the most effective catalyst, we then set about exploring the substrate scope of this manganese complex. In particular, a selection of (hetero)aryl-methyl ketone substrates ere explored in order to gain a deeper understanding of the tolerance of this catalyst to differing electronic and steric properties (Scheme 3).

Besides the initially tested substrate (**1a**: 98% conversion to **2a**), *para*-alkyl substituted derivatives **1b** and **1j** were also shown to give good conversions to the corresponding alcohols (**2b** and **2j**), whereas the mesityl-substituted substrate **1h** showed inferior performance, an observation that is likely due to the additional steric properties of the *ortho*-methyl groups. A clear favourability was identified for fluorine-containing aryl substrates where high conversions to the corresponding alcohol were observed (>98% for **1d–1f**). This could be, in part, due to the powerful electron withdrawing effect of these fluorine atoms across the aryl ring making the carbonyl bond more susceptible to addition of two hydrogen atoms (see later). It is notable that this is not the case for all the halogenated substrates tested with bromide containing substrate **1c** proving rather sluggish. In addition, the one non-methyl aryl ketone examined, CF_3-containing **1m**, showed a considerably lower conversion. Moreover, the *para*-amino bearing **1i** afforded less than 10% conversion which can likely be attributed to the amino-nitrogen undergoing coordination to the catalyst and, hence inhibiting turnover. Perhaps of wider applicability of this catalysis, is its tolerance towards different heterocycles. Notably, the current catalyst saw excellent to moderate conversions to the corresponding alcohols using pyridyl ketone **1k** and thiophene-containing ketone **1n**, respectively. As a more challenging substrate, the ferrocenyl substrate (**1l**) allowed only low conversions to **2l** (7%).

Mechanistic studies

In an attempt to shed light on the catalytic steps followed in these transformations, DFT calculations were employed using **Mn1d** in order to model both (i) an outer-sphere concerted reaction pathway and (ii) a stepwise inner-sphere mechanism based on the conversion of **1a** to **2a**; the former generally being considered the most favoured.[11,28,29,32,33,41,44–47] Scheme 4 shows the proposed outer-sphere pathway using **Mn1d**-I (generated following loss of HBr from **Mn1d**) as the starting point (set at ΔG = 0.0 kcal mol^{-1}). Following interaction of **Mn1d**-I with an incoming isopropanol molecule, **Mn1d**-TS2-OUT is formed as a transition state. Concerted protonation and hydride formation ensues to form hydride intermediate, **Mn1d**-III, which is tentatively supported by a broad hydride resonance at *ca.* δ −5 ppm in the ^{1}H NMR spectrum. **Mn1d**-III can then undergo interaction with acetophenone (**1a**) to form two transition states, **Mn1d**-TS3-OUT-R (21.3 kcal mol^{-1}) in which the phenyl ring of the substrate is positioned above the pyridinol ring and a higher energy transition state (**Mn1d**-TS3-OUT-S, 22.5 kcal mol^{-1}) in which the phenyl group is remote from the pyridinol ring. This small differences in energy can likely be credited to the assistive effect of π–π stacking of the aromatic rings as well as the steric hindrance with the *N*-aryl group. Interestingly the relative energy level of **Mn1d**-TS2-OUT suggests that the largest energy barrier is not in the hydrogen transfer to **1a** (ΔG = 13.3, 12.1 kcal mol^{-1}) but rather the initial formation of the Mn–H species (ΔG = 24.7 kcal mol^{-1}).

The alternative inner sphere pathway is shown in the SI (see Fig. S67) and proceeds in a stepwise manner involving three Mn intermediates. Firstly, **Mn1d**-I is transformed into **INT**-II *via* transfer of the O–H proton from **1a** to the pyridonate unit leading to pyridinol (*via* aromatisation) and isopropoxide formation. β-H elimination and acetone dissociation then gives hydride intermediate, **Mn1d**-III; also found in the outer sphere pathway. Subsequently, transfer of the Mn-hydride in **Mn1d**-III

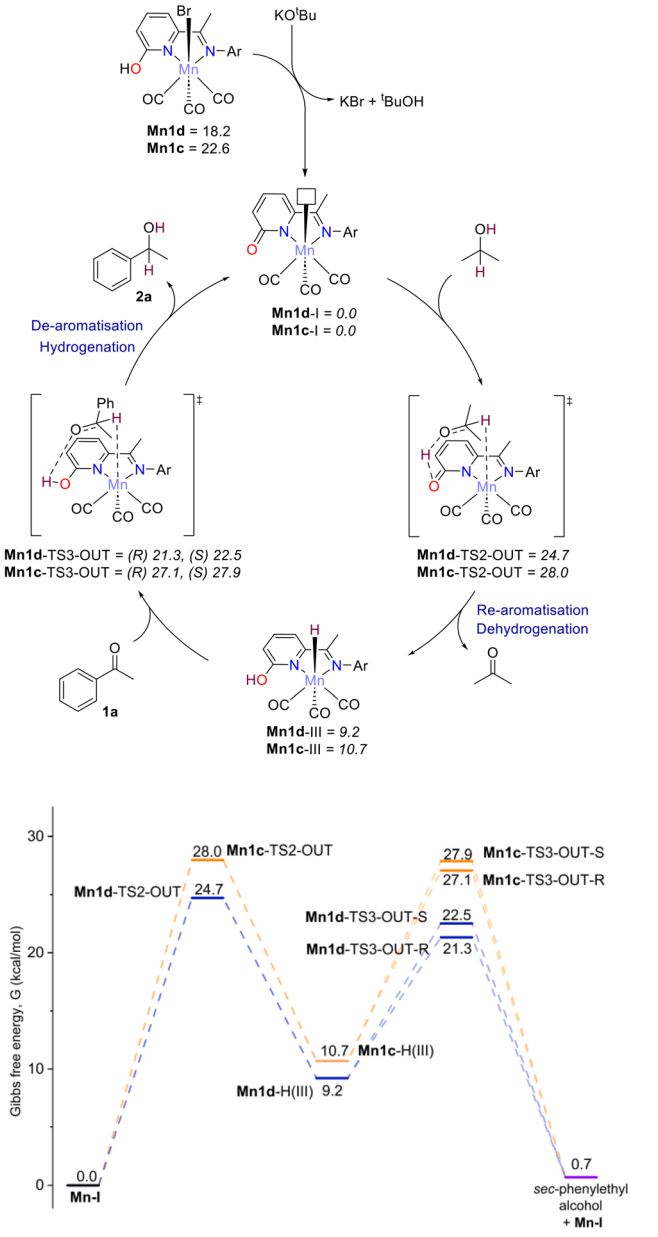

Scheme 5 Catalytic cycle (top) for the transfer hydrogenation of acetophenone (**1a**) for both **Mn1d** and **Mn1c** along with the computed energy profiles (bottom); all ΔG values are in kcal mol^{-1}.

to the carbonyl carbon in **1a** leads to 1-phenylethoxide **INT**-IV (as R and S forms) that can regenerate **Mn1d**-I by loss of **2a**.

Overall, comparison of the two computed pathways reveals a modest difference in the highest energy transition states of 1.5 kcal mol^{-1} (*viz.* **Mn1d**-TS2-IN *vs.* **Mn1d**-TS2-OUT, Fig. S68), with only a minor bias towards the outer sphere pathway. Consequently, an inner-sphere pathway remains plausible; similar conclusions have been reported elsewhere.[28] However, it should be pointed out that solvent-assisted pathways and the requirement for excess base have not been fully accounted for in this mechanistic analysis.[48,49]

As noted earlier, the experimental results indicate that manganese complexes with *N*-aryl groups bearing more sterically bulky *ortho*-substituents were less effective in this transformation (98% for **Mn1d** *vs.* 56% for **Mn1c**). To further probe this observation, DFT calculations were additionally employed using **Mn1c** (*N*-2,4,6-triisopropylphenyl) to compute the corresponding outer-sphere TH pathway. Scheme 5 shows a catalytic cycle that incorporates the highly exergonic initiation step and shows the relative energies for **Mn1**-TS2-OUT and **Mn1**-TS3-OUT for both **Mn1c** and **Mn1d**. In both cases, the values determined for **Mn1c** exceed those found for **Mn1d**, with **Mn1c**-TS2-OUT higher in energy by 3.3 kcal mol^{-1}, while **Mn1c**-TS3-OUT-R and **Mn1c**-TS3-OUT-S are higher by 5.8 and 5.4 kcal mol^{-1} respectively; findings that would suggest that **Mn1**-TS2-out is the rate determining step. Similarly, the ground state for hydride **Mn1**-III is 1.5 kcal mol^{-1} higher in energy for **Mn1c**.

In short, the higher energy barriers for **Mn1**-TS2-OUT and **Mn1**-TS3-OUT for **Mn1c** over **Mn1d** support the experimental findings and highlight the importance of steric factors in the TH. Evidently, the catalytic pocket created by **Mn1d** is more accessible thereby leading to a more effective approach by the substrate.

Conclusions

In summary, five examples of 6-arylimino-2-pyridones, H**L1a**–H**L1e**, have been successfully synthesised using a series of straightforward synthetic steps. Upon reaction with $Mn(CO)_5Br$, the Mn(I) complexes **Mn1a–Mn1e** have been isolated in good yield and fully characterised and reveal the N,N-chelating ligand to adopt the 2-pyridinol form. Likewise, the related *N*,*O*-complex **Mn2** has shown a preference for the 2-pyridinol form. All six complexes exhibited distinct variations in the level of activity for the TH of acetophenone with the least sterically hindered 4-isopropylphenyl-containing **Mn1d** the standout performer and *N*,*O*-bound **Mn2** the poorest. Furthermore, **Mn1d** could mediate the TH of a wide range of substituted (hetero)aryl-methyl ketones with the conversions to the corresponding secondary alcohols influenced by steric/electronic properties of the ketonic substrate. DFT calculations highlight firstly a modest bias toward an outer-sphere mechanistic pathway in line with that found for related Mn(I) catalysts. Secondly, these calculations highlight the detrimental role played by the steric properties on the efficiency of this hydrogenative transformation; a finding that is consistent with the empirical results. Overall, we feel that these results could provide important insights in future catalyst design that may be of relevance to the wider field of (de)hydrogenation.

Experimental details

General methods

All reactions were carried out under standard Schlenk conditions under an atmosphere of nitrogen unless otherwise stated. All solvents used were dried over appropriate drying agents, distilled and stored over molecular sieves and degassed prior to use. All NMR spectra (^1H, ^{13}C) were recorded on a Bruker Avance III 500 MHz spectrometer with a 5 mm BBO probe, Bruker Avance III HD 400 MHz spectrometer with a 5 mm BBO probe or with a Bruker Avance NEO 500 MHz spectrometer with either a 5 mm Prodigy BBO cryoprobe or a 5 mm BBFO probe. All deuterated solvents were purchased from Goss Scientific and Sigma-Aldrich. Infra-red spectra were obtained using a Bruker ALPHA II compact FT-IR spectrometer. High resolution mass spectra were obtained using a Waters G2 XS QTof mass spectrometer equipped with Waters Acquity classic UPLC system. Samples for elemental analysis were weighed using Mettler Toledo high precision scale and analysed using ThermoFlash 2000 at London Metropolitan University. All reagents were obtained from commercial suppliers while the compound 6-bromo-2-methoxypyridine was prepared as described previously.[50]

Synthesis of 6-acetyl-2-methoxypyridine

A 3-neck oven dry round bottom flask equipped with a dropping funnel and charged with a stir bar was placed under an atmosphere of nitrogen. 6-Bromo-2-methoxypyridine (2.906 g, 15.5 mmol, 1 eq.) was added *via* syringe along with THF (40 mL) and cooled to −78 °C. *n*-BuLi (13 mL, 1.6 M in hexanes, 1.3 eq.) was then slowly added to the solution and the mixture stirred for 1 h. Dry dimethylacetamide (1.7 mL, 1.1 eq.) was then added dropwise to the solution and stirred for a further 1 h at −78 °C. After warming to room temperature, the reaction was quenched with aqueous NH_4Cl (25 mL, 20% w/v) and the aqueous layer was subsequently separated and washed with diethyl ether (5 × 25 mL). The combined organic layers were then washed with de-ionised water (2 × 25 mL) and brine (25 mL). The organic layer was then dried over $MgSO_4$ and all volatiles removed under reduced pressure to afford a crude yellow oil. This oil was purified using silica gel chromatography using an eluent system based on 2 : 98 ethyl acetate : petroleum ether to afford the product as a white crystalline material (1.926 g, 79%). The ^1H NMR data obtained were consistent with that reported in the literature.[51] ^1H NMR (500 MHz, $CDCl_3$, 298 K): δ 7.69 (dd, J = 7.3, 8.2 Hz, 1H, Py–H), 7.63 (dd, J = 0.9, 7.2 Hz, 1H, Py–H), 6.93 (dd, J = 0.9, 8.2 Hz, 1H, Py–H), 4.00 (s, 3H, OCH_3), 2.68 (s, 3H, CCH_3). HRMS (ESI+, MeOH): calc. for $C_8H_{10}NO_2$ [M + H] 152.0712, found 152.0712.

Synthesis of 6-acetyl-pyridin-2-one

2-Methoxy-6-acetyl pyridine (2.035 g, 14.8 mmol) was added to a 100 mL round bottom flask equipped with a condenser and a stir bead. Concentrated HBr (36 mL, 33% in AcOH) was added and the mixture heated to 110 °C for 4 h. After cooling to room temperature, the solution was carefully neutralised with aqueous NaOH (4 M) and washed with diethyl ether (4 × 125 mL). The aqueous layer was then dried under reduced pressure and the resulting residue ground into a powder. This was then extracted with acetone (6 × 75 mL) and dried under reduced pressure to give a beige solid (1.815 g, 99%). The ^{1}H NMR data obtained were consistent with that reported in the literature.[52] ^{1}H NMR (500 MHz, $CDCl_3$, 298 K): δ 9.57–9.44 (br s, 1H, NH), 7.48 (dd, J = 6.7, 9.3 Hz, 1H, Py–H), 6.88 (d, J = 6.6 Hz, 1H, Py–H), 6.83 (d, J = 9.3 Hz, 1H, Py–H), 2.55 (s, 3H, CCH_3). ^{13}C NMR (126 MHz, $CDCl_3$, 298 K) δ 190.4 (1C, *C*═O), 161.6 (1C, *C*–OH), 139.5 (1C, N*C*C), 138.6 (1C, *C*H), 128.1 (1C, *C*H), 109.7 (1C, *C*H), 24.5 (1C, C*C*H$_3$). HRMS (ESI+, MeOH): calc. for $C_7H_8NO_2$ [M + H] 138.0555, found 138.0555, calc. for $C_7H_8NO_2Na$ [M + Na] 160.0376, found 160.374. FT-IR ν_{max}/cm^{-1} 3094br (NH), 2989w (CH), 1685m (CO), 1643s (CO), 1599s (CC), 1433m (CH), 1245m (CO), 798 (CC).

Synthesis of 6-(1-(arylimino)ethyl)pyridin-2(1*H*)-ones (HL1a–HL1e)

General procedure: 6-acetyl-pyridin-2-one (0.494 g, 3.60 mmol) was added to a 50 mL round bottom flask containing the corresponding aniline (5.36 mmol, 1.5 eq.), *p*-toluene-sulfonic acid (0.01 eq.) and *n*-butanol (10 mL, *ca.* 0.35 M of 6 acetyl-pyridin-2-one). The flask was then fitted with a Dean Stark apparatus and condenser. The mixture was stirred and heated to reflux for 72 h. Once cooled to room temperature, all volatiles were removed under reduced pressure and the resulting oil purified *via* silica column chromatography eluting with 100% ethyl acetate to give the product as a yellow solid.

Aryl = 2,6-diisopropylphenyl (HL1a). Following the general procedure described above with the same molar ratios, H**L1a** was isolated as a yellow powder (0.672 g, 63%). The ^{1}H NMR data obtained were consistent with that reported in the literature.[53] ^{1}H NMR (400 MHz, $CDCl_3$, 298 K): δ 10.34 (br s, 1H, OH), 7.50 (dd, J = 6.7, 9.1 Hz, 1H, Py–H), 7.19–7.10 (m, 3H, Ar–H), 6.77 (d, J = 9.2 Hz, 1H, Py–H), 6.66 (d, J = 6.7 Hz, 1H, Py–H), 2.57 (quin, J = 6.9 Hz, 2H, CH), 2.01 (s, 3H, CCH_3), 1.12 (d, J = 6.9 Hz, 12H, CH_3). ^{13}C NMR (101 MHz CD_3SOCD_3, 298 K) δ (162.5, 1C, N═*C*CH$_3$), (145.1, 1C, *C*═O), (141.1, 1C, N*C*C), 140.5 (1C, N*C*C), 139.1 (2C, *C*H), 136.0 (1C, *C*H), 128.5 (1C, *C*H) 124.7 (1C, *C*H), 123.5 (2C, *C*H), 114.4 (1C, *C*H), 28.1 (1C, C*C*H), 26.0 (1C, C*C*H), 23.6 (2C, *C*H$_3$), 23.2 (2C, *C*H$_3$), 16.9 (1C, N═C*C*H$_3$). HRMS (ESI+, MeOH): found: 297.1967, calc. for $C_{19}H_{25}N_2O$ [M + H] 297.1967 FT-IR ν_{max}/cm^{-1} 3128br (OH), 2959w (CH), 1650vs (C═N) 1597s (CH), 1450w (CH), 1431w (CH), 1285m (CO), 978 m (CN), 801s (CC), 562 m (CC).

Aryl = 4-bromo-2,6-diisopropylphenyl (HL1b). Following the general procedure described above with the same molar ratios, H**L1b** was isolated as a yellow powder (1.120 g, 85%). ^{1}H NMR (400 MHz, $CDCl_3$, 298 K): δ 10.17 (s, 1H, OH), 7.42 (t, J = 8 Hz, 1H, Py–H), 7.19 (s, 2H, Ar–H), 6.70 (1H, d, J = 8.6 Hz, Py–H), 6.59 (d, J = 6.8 Hz, 1H, Py–H), 2.46 (sept, J = 6.8 Hz, 2H, CH), 1.94 (s, 3H, CCH_3), 1.04 (d, J = 6.9 Hz, 12H, CH_3). ^{13}C NMR (101 MHz, CD_3SOCD_3, 298 K): δ 162.2 (1C, N═*C*CH$_3$), 144.5 (1C, *C*═O), 140.9 (2C, N*C*C), 139.0 (3C, *C*H), 126.4 (2C, *C*H), 117.3 (1C, *C*H), 109.0 (1C, *C*H), 28.3 (2C, C*C*H), 23.3 (2C, *C*H$_3$), 22.9 (2C, *C*H$_3$), 16.9 (1C, N═C*C*H$_3$). HRMS (TOF + ESI, MeOH), found: 375.1066, calc. for $C_{19}H_{23}N_2OBr$ [M] 375.1072. FT-IR ν_{max}/cm^{-1} 3090br (OH), 2963w (CH), 1630vs (C═N) 1592s (CH), 1456w (CH), 1440w (CH), 1283m (CO), 980w (CN), 863s (CC) 797s (CBr), 562 m (CC).

Aryl = 2,4,6-triisopropylphenyl (HL1c). Following the general procedure described above with the same molar ratios, H**L1c** was isolated as a yellow powder (1.024 g, 84%). ^{1}H NMR (400 MHz, $CDCl_3$, 298 K): δ 10.34 (s, 1H, OH), 7.49 (dd, J = 6.8, 9.3 Hz, 1H, Py–H), 6.99 (s, 2H, Ar–H), 6.75 (dd, J = 1.5, 9.2 Hz, 1H, Py–H), 6.65 (d, J = 7.1 Hz, 1H Py–H), 2.89 (sept, J = 6.9 Hz, 1H, CH) 2.54 (sept, J = 6.9 Hz, 2H, CH), 2.01 (s, 3H, CCH_3), 1.27 (d, J = 7.0 Hz, 6H, CH_3), 1.11 (dd, J = 0.9, 6.9 Hz, 12H, CH_3). ^{13}C NMR (100 MHz; $CDCl_3$, 298 K): δ 162.8 (1C, N═*C*CH$_3$), 158.3 (1C, CH), 145.3 (1C, *C*═O), 142.3 (1C, N*C*C), 141.2 (1C, *C*CH), 140.5 (1C, *C*H), 136.1 (2C, N*C*C), 125.3 (2C, *C*H), 121.4 (1C, *C*H), 107.1 (1C, *C*H), 34.4 (1C, *C*HCH$_3$), 28.8 (2C, *C*HCH$_3$), 24.6 (2C, *C*H$_3$), 23.8 (2C, *C*H$_3$), 23.3 (2C, *C*H$_3$), 16.3 (1C, N═C*C*H$_3$). HRMS (TOF): calculated for $C_{22}H_{31}N_2O$ [M + H], 339.2436, found: 339.2430. FT-IR ν_{max}/cm^{-1} 3175br (OH), 2957w (CH), 1656vs (C═N) 1602vs (CH), 1452m (CH), 1431w (CH), 1289w (CO), 1007w (CN), 801s (CC), 562 m (CC).

Aryl = 4-isopropylphenyl (HL1d). Following the general procedure described above with the same molar ratios, H**L1d** was isolated as a yellow powder (0.639 g, 70%). ^{1}H NMR (400 MHz, $CDCl_3$, 298 K) δ 10.30 (br s, 1H, OH), 7.46 (dd, J = 7.0, 8.8 Hz, 1H, Py–H), 7.24 (d, J = 8.1 Hz, 2H, Ar–H), 6.73 (m, J = 8.3 Hz, 1H, Py–H, 2H Ar–H), 6.64 (d, J = 7.0 Hz, 1H, Py–H), 2.85 (spt, J = 6.9 Hz, 1H, CH), 2.21 (s, 3H, CH_3), 1.19 (d, J = 6.9 Hz, 6H, CH_3). ^{13}C NMR (101 MHz, $CDCl_3$, 298 K): δ 155.7 (1C, N═*C*CH$_3$), 145.2 (1C, *C*═O), 144.6 (1C, N*C*C), 140.5 (1C, *C*–CH), 139.1 (1C, *C*H), 126.0 (2C, *C*H), 123.6 (2C, *C*H), 119.0 (1C, *C*H), 114.4 (1C, *C*H), 105.8 (1C, *C*H), 32.6 (1C, C*C*H), 23.2 (1C, *C*H$_3$), 23.0 (1C, *C*H$_3$), 14.1 (1C, N═C*C*H$_3$). HRMS (ESI+, MeOH): calc. for $C_{16}H_{18}N_2O$ [M + H] 255.1497, found 255.1498. Calc. for $C_{16}H_{18}N_2ONa$ [M + Na] 277.1317, found 277.1319. FT-IR ν_{max}/cm^{-1} 3314br (OH), 2955w (CH), 1648vs (C═N) 1598s (CH), 1450w (CH), 1440w (CH), 1291m (CO), 1011m (CN), 795s (CC), 550m (CC).

Aryl = 2,4,6-trimethylphenyl (HL1e). Following the general procedure described above with the same molar ratios, H**L1e** was isolated as a dark yellow powder (0.867 g, 90%). ^{1}H NMR (400 MHz, $CDCl_3$, 298 K): δ 10.35 (br s, 1H, OH), 7.48 (dd, J = 6.8, 9.3 Hz, 1H, Py–H), 6.88 (s, 2H, Ar–H), 6.74 (d, J = 9.2 Hz, 1H, Py–H), 6.64 (d, J = 6.7 Hz, 1H, Py–H), 2.29 (s, 3H, Ar–H), 1.98 (s, 3H, CCH_3), 1.93 (s, 6H, Ar–H). ^{13}C NMR (101 MHz, $CDCl_3$, 298 K): δ 157.9 (1C, *C*═N), 144.2 (1C, *C*–OH), 140.8 (1C, *C*–N), 140.0 (1C, *C*–N), 133.4 (1C, *C*H), 128.7 (3C, *C*H), 125.4 (1C, *C*CH$_3$), 125.0 (1C, *C*CH$_3$), 106.6 (1C, *C*H), 20.7 (1C, *C*H$_3$),

17.9 (1C, *C*H$_3$), 15.3 (1C, N=C*C*H$_3$). HRMS (ESI+, MeOH): calc. for $C_{16}H_{18}N_2O$ [M + H] 255.1497, found 255.1497. Calc. for $C_{16}H_{18}N_2ONa$ [M + Na] 277.1319, found 277.1317. FT-IR ν_{max}/cm^{-1} 3144br (OH), 2972w (CH), 1633vs (C=N) 1600s (CH), 1475w (CH), 1454w (CH), 1287w (CO), 1007m (CN), 980m (CN), 816s (CC), 554m (CC).

Synthesis of [2-OH-6-{CMe=N(Ar)}C$_5$H$_3$N]MnBr(CO)$_3$ (Mn1a–Mn1e)

General procedure: a small oven dried Schlenk flask, equipped with a stir bead, was evacuated and backfilled with nitrogen. The flask was charged with an equimolar amounts of H**L1** and Mn(CO)$_5$Br and dissolved in the corresponding solvent (0.1 M solution). This solution was then stirred in darkness at 30 °C for 18 h. The resulting precipitate was filtered and washed with hexane to give the product as an orange solid.

Ar = 2,6-^{i}Pr$_2$C$_6$H$_3$ (Mn1a). Following the general procedure described above, H**L1a** (88.0 mg, 0.3 mmol) and Mn(CO)$_5$Br (82.0 mg, 0.3 mmol) were dissolved in diethyl ether (3 mL). The resulting precipitate was washed with diethyl ether (1 × 10 mL) and hexane (2 × 5 mL) affording **Mn1a** as an orange solid (81.3 mg, 53%). ^{1}H NMR (400 MHz, CD$_3$SOCD$_3$, 298 K) δ 12.76–13.75 (m, 1H, OH), 8.05 (t, J = 7.84 Hz, 1H, Py–H), 7.79 (d, J = 7.52 Hz, 1H, Py–H), 7.34 (t, J = 7.10 Hz, 3H, Ar–H), 7.16 (d, J = 8.25 Hz, 1H, Py–H), 3.67 (quin, J = 6.80 Hz, 1H, CH), 2.80 (quin, J = 7.40 Hz, 1H, CH), 2.30 (s, 3H N=CCH$_3$), 1.25 (br d, J = 6.60 Hz, 3H, CCH$_3$), 1.22 (br d, J = 6.42 Hz, 3H, CCH$_3$), 1.01 (br d, J = 6.69 Hz, 6H, CCH$_3$). ^{13}C NMR (126 MHz, CD$_3$SOCD$_3$, 298 K): δ 222.9 (1C, *C*≡O), 222.3 (1C, *C*≡O), 220.9 (1C, *C*≡O), 177.2 (1C, *C*=N), 165.1 (1C, *C*–OH), 153.5 (1C, *C*–N), 145.5 (1C, *C*–N), 141.0 (1C, *C*H), 139.9 (1C, *C*H), 138.3 (1C, *C*CH), 127.3 (1C, *C*H), 124.8 (1C, *C*H), 124.3 (1C, CH), 119.7 (1C, *C*H), 114.0 (1C, *C*H), 27.4 (2C, C*C*H), 25.0 (1C, *C*H$_3$), 24.9 (1C, *C*H$_3$), 24.6 (1C, *C*H$_3$), 24.3 (1C, *C*H$_3$), 24.2 (1C, *C*H$_3$), 19.7 (1C, N=C*C*H$_3$). HRMS (ESI−, MeOH): calc. for $C_{22}H_{23}N_2O_4Mn^{79}Br$ [M − H]$^-$ 513.0220, found 513.0220. Calc. for $C_{19}H_{23}N_2OMn^{79}Br$ [M − H–3(CO)]$^-$ 429.0374, found 429.0376. FT-IR ν_{max}/cm^{-1} 3062w (OH), 2961w (CH), 2018vs (CO), 1937vs (CO), 1903vs (CO), 1633m (CN), 1592s (CH), 1458w (CH), 1440w (CH), 1260m (CO), 1096m (CN), 1013s (CN) 801vs (CC), 630s (CC). Elemental analysis calc. for $C_{22}H_{23}N_2O_4MnBr$ (0.25Et$_2$O) C, 51.8; H, 5.0; N 5.3 found C, 51.5; H, 5.3; N, 5.2.

Ar = 2,6-^{i}Pr$_2$-4-BrC$_6$H$_2$ (Mn1b). Following the general procedure above, H**L1b** (113.0 mg, 0.3 mmol) and Mn(CO)$_5$Br (83.0 mg, 0.3 mmol) were dissolved in diethyl ether (3 mL). On completion of the reaction, the solvent was concentrated under reduced pressure and hexane (5 mL) added to induce precipitation. The solid was filtered and washed with diethyl ether (1 × 10 mL) and hexane (2 × 5 mL), to afford **Mn1b** as an orange solid (130 mg, 73%). ^{1}H NMR (400 MHz, CD$_3$SOCD$_3$, 298 K): δ 13.33 (br, s, 1H, OH), 8.04 (t, J = 7.91 Hz, 1H, Py–H), 7.80 (d, J = 7.41 Hz, 1H, Py–H), 7.49 (s, 2H, Ar–H), 7.17 (d, J = 8.31 Hz, 1H, Py–H), 3.64 (quin, J = 6.75 Hz, 1H), 2.76 (quin, J = 6.41 Hz, 1H), 2.31 (s, 3H, N=CCH$_3$), 1.23 (br d, J = 6.62 Hz, 3H, CCH$_3$), 1.19 (br d, J = 6.28 Hz, 3H, CCH$_3$), 1.01 (br d, J = 6.51 Hz, 6H, CCH$_3$). ^{13}C NMR (126 MHz, CD$_3$SOCD$_3$, 298 K): δ 222.9 (1C, C≡O), 222.5 (1C, C≡O), 220.9 (1C, C≡O), 178.1 (1C, *C*=N), 165.2 (1C, *C*–OH), 153.4 (1C, *C*–N), 144.9 (1C, *C*–N), 143.2 (1C, *C*H), 141.6 (1C, *C*H), 141.2 (1C, *C*CH), 127.9 (1C, *C*H), 127.5 (1C, *C*H), 120.5 (1C, CH), 120.3 (1C, *C*H), 114.3 (1C, *C*H), 27.8 (1C, C*C*H), 27.8 (C, C*C*H), 24.8 (1C, *C*H$_3$), 24.7 (1C, *C*H$_3$), 24.4 (1C, *C*H$_3$), 24.1 (1C, *C*H$_3$), 20.0 (1C, N=C*C*H$_3$). HRMS (ESI−, MeOH): calc. for $C_{22}H_{23}N_2O_4Mn^{79}Br$ [M − H]$^-$ 513.0220, found 513.0220. Calc. for $C_{19}H_{23}N_2OMn^{79}Br$ [M − H–3(CO)]$^-$ 429.0374, found 429.0376. FT-IR ν_{max}/cm^{-1} 3062w (OH), 2961w (CH), 2018vs (CO), 1937vs (CO), 1903vs (CO), 1633m (CN), 1592s (CH), 1458w (CH), 1440w (CH), 1260m (CO), 1096m (CN), 1013s (CN) 801vs (CC), 630s (CC). Elemental analysis calc. for $C_{22}H_{23}Br_2MnN_2O_4$ (0.25CH_2Cl_2) C, 43.3; H, 3.9; N 4.6 found C, 43.2; H, 4.0; N, 4.3.

Ar = 2,4,6-^{i}Pr$_3$C$_6$H$_2$ (Mn1c). Following the general procedure described above, H**L1c** (206.0 mg, 0.6 mmol) and Mn(CO)$_5$Br (166.0 mg, 0.6 mmol) were dissolved in hexane (6 mL) and the reaction mixture stirred and heated to reflux for 18 h. Once cooled to room temperature, a suspension was formed and collected by gravity filtration and washed with hexane (5 × 20 mL) affording **Mn1c** as an orange solid (264 mg, 78%). ^{1}H NMR (400 MHz, CD$_3$SOCD$_3$, 298 K): δ 13.17 (br s, 1H, OH), 8.03 (t, J = 7.84 Hz, 1H, Py–H), 7.80 (d, J = 7.20 Hz, 1H, Py–H), 7.16 (m, 3H, Ar–H, Py–H), 3.64 (quin, J = 6.64 Hz, 1H), 2.93 (quin, J = 6.84 Hz, 1H), 2.77 (quin, J = 6.41 Hz, 1H), 2.27 (s, 3H, N=CCH$_3$), 1.22 (br d, J = 5.84 Hz, 6H, CCH$_3$), 1.21 (br d, J = 6.07 Hz, 6H, CCH$_3$), 1.00 (br d, J = 6.84 Hz, 6H, CCH$_3$). ^{13}C NMR (126 MHz, CD$_3$SOCD$_3$, 298 K): δ 222.4 (1C, *C*≡O), 221.6 (1C, *C*≡O), 220.4 (1C, *C*≡O), 176.0 (1C, *C*=N), 164.6 (1C, *C*–OH), 153.0 (1C, *C*–N), 146.1 (1C, *C*–N), 143.0 (1C, *C*CH), 140.3 (1C, *C*CH), 138.9 (1C, *C*CH), 137.3 (1C, *C*H), 121.6 (1C, *C*H), 121.2 (1C, *C*H), 119.5 (1C, *C*H), 113.3 (1C, *C*H), 32.4 (1C, C*C*H), 26.7 (1C, C*C*H), 24.4 (1C, C*C*H), 24.2 (1C, *C*H$_3$), 24.0 (1C, *C*H$_3$), 23.7 (1C, *C*H$_3$), 23.2 (2C, *C*H$_3$), 19.1 (1C, N=C*C*H$_3$). HRMS (ESI$^-$, MeOH): calc. for $C_{25}H_{29}N_2O_4Mn^{79}Br$ [M − H]$^-$ 555.0691, found 555.0691. Calc. for $C_{22}H_{29}N_2OMn^{79}Br$ [M − H–3(CO)]$^-$ 471.0844, found 471.0847. FT-IR ν_{max}/cm^{-1} 3101br (OH), 2961w (CH), 2018s (CO), 1940s (CO), 1903s (CO), 1637m (CN), 1590m (CH), 1458w (CH), 1440w (CH), 1258m (CO), 1100w (CN), 1011w (CN) 803vs (CC), 626s (CC).

Ar = 4-^{i}PrC$_6$H$_4$ (Mn1d). Following the general procedure described above, H**L1d** (258.3 mg, 1.02 mmol) and Mn(CO)$_5$Br (278.1 mg, 1.02 mmol) were dissolved in dichloromethane (10 mL). The resulting solid was filtered and washed with dichloromethane (10 mL) and diethyl ether (3 × 10 mL) to afford **Mn1d** as an orange solid (349 mg, 74%). ^{1}H NMR (500 MHz, CD$_3$SOCD$_3$, 298 K): δ 12.45 (br s, 1H, OH), 8.02 (br t, J = 7.7 Hz, 1H, Py–H), 7.77 (br d, J = 7.1 Hz, 1H, Py–H), 7.41 (br d, J = 7.9 Hz, 2H, Ar–H), 7.28 (br s, 1H, Ar–H), 7.13 (br d, J = 8.3 Hz, 1H, Py–H), 7.04 (br s, 1H, Ar–H), 2.97 (quin, J = 6.2 Hz, 1H, CH), 2.29 (s, 3H, CCH$_3$), 1.26 (d, J = 6.7 Hz, 6H, CH$_3$) ^{13}C NMR (126 MHz, CD$_3$SOCD$_3$, 298 K): δ 222.7 (1C, *C*≡O), 221.8 (1C, *C*≡O), 220.5 (1C, *C*≡O), 174.4 (1C, *C*=N), 165.3 (1C, *C*–OH), 154.0 (1C, *C*–N), 149.2 (1C, *C*CH), 146.6 (1C, *C*–N), 140.9 (2C, *C*H), 127.0 (2C, *C*H), 119.4 (1C, *C*H), 113.7 (1C, *C*H), 32.9 (1C,

C*C*H), 23.8 (1C, *C*H$_3$), 23.7 (1C, *C*H$_3$), 18.0 (1C, N=C*C*H$_3$). HRMS (ESI$^-$, MeOH): calc. for $C_{19}H_{17}N_2O_4Mn^{79}Br$ [M − H]$^-$ 470.9752, found 470.9755. Calc. for $C_{16}H_{17}N_2OMn^{79}Br$ [M − H–3(CO)]$^-$ 386.9905, found 386.9911. FT-IR ν_{max}/cm^{-1} 3114w (OH), 2959w (CH), 2024vs (CO), 1940vs (CO), 1904vs (CO), 1604m (CN), 1462w (CH), 1332w (CH), 1260m (CO), 1094m (CN), 1054m (CN), 1019m (CN) 809s (CC), 628s (CC). Elemental analysis calc. for $C_{19}H_{18}N_2BrO_4Mn$ (0.25CH_2Cl_2) C, 46.8; H, 3.8; N 5.7 found C, 46.8; H, 3.6; N, 5.6.

Ar = 2,4,6-Me$_3$C$_6$H$_2$ (Mn1e). Following the general procedure described above, H**L1e** (25.4 mg, 0.1 mmol) and Mn(CO)$_5$Br (28.1 mg, 0.1 mmol) were dissolved in dichloromethane (1 mL). The resulting precipitate was filtered and washed with dichloromethane (2 mL) and hexane (3 × 10 mL) affording **Mn1e** as an orange solid (22.8 mg, 48%). ^{1}H NMR (500 MHz, CD_3SOCD_3, 298 K): δ 13.11 (br s, 1H, OH), 8.04 (t, J = 7.9 Hz, 1H, Py–H), 7.79 (d, J = 7.3 Hz, 1H, Py–H), 7.14 (d, J = 8.3 Hz, 1H, Py–H), 7.01 (s, 2H, Ar–H), 2.40 (s, 3H, CH_3), 2.29 (s, 3H, CH_3), 2.23 (s, 3H, CH_3), 2.04 (s, 3H, CH_3). ^{13}C NMR (126 MHz, CD_3SOCD_3, 298 K): δ 222.6 (1C, *C*≡O), 222.4 (1C, *C*≡O), 221.3 (1C, *C*≡O), 176.9 (1C, *C*=N), 165.2 (1C, *C*–OH), 153.7 (1C, *C*–N), 146.5 (1C, *C*–N), 141.1 (1C, *C*H), 135.2 (1C, *C*CH$_3$), 129.3 (1C, *C*H), 129.3 (1C, *C*H), 129.2 (1C, *C*CH$_3$), 126.9 (1C, *C*CH$_3$), 119.6 (1C, *C*H), 113.8 (1C, *C*H), 20.5 (1C, *C*H$_3$), 20.3 (1C, *C*H$_3$), 18.0 (1C, *C*H$_3$), 17.7 (1C, N=C*C*H$_3$). HRMS (ESI−, MeOH): calc. for $C_{19}H_{17}N_2O_4Mn^{79}Br$ [M − H]$^-$ 470.9752, found 470.9747. Calc. for $C_{16}H_{17}N_2OMn^{79}Br$ [M − H–3(CO)]$^-$ 386.9905, found 386.9889 FT-IR ν_{max}/cm^{-1} 3093br (OH), 2979br (CH), 2020s (CO), 1940s (CO), 1897vs (CO), 1596m (CN), 1472w (CH), 1370m (CH),1326w (CH), 1260m (CO), 1015w (CN) 809s (CC), 680m (CC), 628s (CC). Elemental analysis calc. for $C_{19}H_{18}N_2BrO_4Mn$ (0.75CH_3OH) C, 47.7; H, 4.3; N 5.6 found C, 47.9; H, 4.6; N, 5.4.

Synthesis of [2-OH-6-(CMe=O)C$_5$H$_3$N]MnBr(CO)$_3$ (Mn2)

A small oven dried Schlenk flask, equipped with a stir bead, was evacuated and backfilled with nitrogen. The flask was charged with an equimolar amounts of 6-acetyl-pyrid-2-one (41.7 mg, 0.3 mmol) and Mn(CO)$_5$Br (82.1 mg, 0.3 mmol) and dissolved in dichloromethane (3 mL). This solution was then stirred in darkness at 30 °C for 18 h. The resulting precipitate was then filtered, washed with dichloromethane (6 mL) and hexane (2 × 5 mL) and then dried under reduced pressure to afford **Mn2** as a brick red solid (61.8 mg, 58%). ^{1}H NMR (500 MHz, CD_3SOCD_3, 298 K) δ (ppm) = 13.35 (br s, 1H, OH), 8.18–8.07 (m, 2H, Py–H), 7.28 (dd, J = 3.1, 6.3 Hz, 1H, Py–H), 2.83 (s, 3H, O=C*C*H$_3$). **Mn2**(DMSO) (40%): 11.03 (br s, 1H, OH), 7.65 (br s, 1H, Py–H), 7.18 (br s, 1H, Py–H), 6.74 (br s, 1H, Py–H), 2.83 (s, 3H, O=C*C*H$_3$). ^{13}C NMR (126 MHz, CD_3SOCD_3): δ 225.6 (s, 1C, *C*≡O), 223.4 (1C, *C*≡O), 219.3 (1C, *C*≡O), 210.8 (1C O*C*CH$_3$), 165.5 (1C, *C*H), 149.5 (1C, *C*H), 141.3 (1C, *C*H), 122.1 (1C, *C*H), 117.1 (1C, *C*H), 25.9 (1C, *C*H$_3$). HRMS (ESI−, MeOH): calc. for $C_{10}H_6NO_5Mn^{79}Br$ [M − H]$^-$, 353.8810, found 353.8806; calc. for $C_7H_6NO_2Mn^{79}Br$ [M − H–3(CO)]$^-$ 269.8962, found 269.8961. Elemental analysis calc. for $C_{10}H_6NO_5MnBr$ C, 33.7; H, 2.0; N 3.9 found C, 33.9; H, 2.1; N, 3.9.

Catalytic protocol employed for the transfer hydrogenation

(a) General procedure for screening **Mn1a–Mn1e** and **Mn2** for the TH of acetophenone (**1a**). An oven dry 20 mL Schlenk flask, equipped with a micro stir bar, was evacuated and backfilled with nitrogen. To this a pre-determined amount of base was added and the flask re-evacuated before being backfilled with nitrogen. Dry ^{i}PrOH (5 mL) was then added and the vessel stirred to dissolve/suspend the base in solution. The corresponding mol% of manganese complex was then added and the mixture stirred to form the active species. The substrate was then added (2 mmol) and the reaction surrounded in foil and placed into an oil bath set at 80 °C and the mixture left stir at this temperature for 24 h with the tap open to the bubbler. After cooling to room temperature, the mixture was diluted with dichloromethane (5 mL) and passed through a silica pipette filter eluting with dichloromethane. A sample of this solution was withdrawn and all volatiles removed under reduced pressure. The spectroscopic conversion of the substrate was then measured using ^{1}H NMR spectroscopy in $CDCl_3$.

(b) General procedure for screening substrates **1a–1n** using **Mn1a**. An oven dry 20 mL Schlenk flask, equipped with a micro stir bar, was evacuated and backfilled with nitrogen. To this K^{t}BuO (7.0 mg, 0.06 mmol, 3 mol%) was added and the flask re-evacuated before being backfilled with nitrogen. Dry ^{i}PrOH (5 mL) was then added and the vessel stirred to dissolve/suspend the K^{t}BuO in solution. **Mn1d** (4.7 mg, 0.01 mmol, 0.5 mol%) was then added and the mixture stirred to form the active species as a red solution. The substrate was then added (2 mmol) and the reaction surrounded in foil and placed into an oil bath set at 80 °C and the mixture left stir at this temperature for 24 h with the tap open to the bubbler. After cooling to room temperature, the mixture was diluted with dichloromethane (5 mL) and passed through a silica pipette filter eluting with dichloromethane. A sample of this solution was withdrawn and all volatiles removed under reduced pressure. The spectroscopic conversion of the substrate was then measured using ^{1}H NMR spectroscopy in $CDCl_3$.

Computational methods

All the calculations were performed at B3LYP-D3(BJ)[54,55] method using ORCA 6.0.1 software package.[56,57] For Mn, the def2-TZVP[58] with the auxiliary def2/J[59] basis sets were used. The Br atom was treated with the 6-311+g(d,p)[60–62] basis set, while the remaining atoms (C, H, N, and O) were described using the 6-31+G(d,p)[51–63] basis set. Structures were optimized using the SMD implicit solvation model, with isopropanol as the solvent.[64] Harmonic vibration frequency calculations were used to confirm the stationary points and to obtain thermodynamic data. The 3D representations of the optimized structures were generated by CYLview20.[65]

Author contributions

S. J. Prettyman was responsible for the data curation, investigation validation and writing. M. H. Alhalafi was involved in some of the initial synthetic work. G. A. Solan was responsible for the supervision, funding acquisition, conceptualisation and writing – review and editing. K. Singh was responsible for the collection of the XRD data, while Dr S. Alqahtani performed the computational investigation.

Conflicts of interest

There are no conflicts to declare.

Data availability

The data supporting this article have been included as part of the supplementary information (SI). Supplementary information: figures and additional characterisation data for ligands, complexes and products of catalysis; coordinates of all optimised structures by DFT calculations. See DOI: https://doi.org/10.1039/d6dt00709k.

CCDC 2540706–2540715 for **Mn1a–Mn1e**, **Mn2**, **Mn1b′**, **Mn1d′**, **HL1a** and **HL1e** contain the supplementary crystallographic data for this paper.[66a–j]

Acknowledgements

The University of Leicester is thanked for financial support and the provision of a studentship to SJP. The EPSRC are acknowledged for grant EP/W02151X/1.

References

1 R. Mondal, A. K. Guin, G. Chakraborty and N. D. Paul, *Org. Biomol. Chem.*, 2022, **20**, 296–328.
2 J. Rana, S. T. Sahoo and P. Daw, *Tetrahedron*, 2021, **99**, 132473.
3 K. Das, S. Waiba, A. Jana and B. Maji, *Chem. Soc. Rev.*, 2022, **51**, 4386–4464.
4 D. Fu, Z. Wang, Q. Liu, S. J. Prettyman, G. A. Solan and W.-H. Sun, *ChemCatChem*, 2024, **16**, e202301567.
5 O. R. Luca and R. H. Crabtree, *Chem. Soc. Rev.*, 2013, **42**, 1440–1459.
6 J. I. van der Vlugt and J. N. H. Reek, *Angew. Chem., Int. Ed.*, 2009, **48**, 8832–8846.
7 H. Grützmacher, *Angew. Chem., Int. Ed.*, 2008, **47**, 1814–1818.
8 L. Alig, M. Fritz and S. Schneider, *Chem. Rev.*, 2019, **119**, 2681–2751.
9 (*a*) Z. Wang, Y. Wang, Q. Lyu, D. Zhu, Z. Ma, B. Gansukh, L. Li, H. Liu, N. Ma and Z. Wang, *J. Catal.*, 2025, **444**, 115998; (*b*) R. Yang, U. Bandyopadhyay, S. Mallet-Ladeira, R. Poli, E. Manoury and A. Labande, *New J. Chem.*, 2026, **50**, 47–57; (*c*) J. A. Fuentes and M. L. Clarke, *Eur. J. Inorg. Chem.*, 2026, **29**, e202500884; (*d*) B. Li, J. Zhang, Y. Ding, D. Ji, Z. Lu, G. Yang, S. Zhang and H. Nie, *Adv. Synth. Catal.*, 2025, **367**, e70011; (*e*) J. Yang, L. Yao, Z. Wang, Z. Zuo, S. Liu, P. Gao, M. Han, Q. Liu, G. A. Solan and W.-H. Sun, *J. Catal.*, 2023, **418**, 40–50; (*f*) H. Jayaprakash, *Dalton Trans.*, 2021, **50**, 14115–14119; (*g*) K. Z. Demmans, M. E. Olson and R. H. Morris, *Organometallics*, 2018, **37**, 4608–4618; (*h*) M. B. Widegren, G. J. Harkness, A. M. Z. Slawin, D. B. Cordes and M. L. Clarke, *Angew. Chem., Int. Ed.*, 2017, **56**, 5825–5828.
10 (*a*) G. Liu, Z. Fu, F. Chen, C. Xu, M. Li and N. Liu, *Chin. J. Chem.*, 2023, **43**, 629; (*b*) S. J. P. Spall, T. Keane, J. Tory, D. C. Cocker, H. Adams, H. Fowler, A. J. H. M. Meijer, F. Hartl and J. A. Weinstein, *Inorg. Chem.*, 2016, **55**, 12568–12582; (*c*) F. Franco, M. F. Pinto, B. Royo and J. Lloret-Fillol, *Angew. Chem., Int. Ed.*, 2018, **57**, 4603–4606; (*d*) R. Van Putten, J. Benschop, V. J. De Munck, M. Weber, C. Müller, G. A. Filonenko and E. A. Pidko, *ChemCatChem*, 2019, **11**, 5232–5235; (*e*) R. Buhaibeh, O. A. Filippov, A. Bruneau-Voisine, J. Willot, C. Duhayon, D. A. Valyaev, N. Lugan, Y. Canac and J. Sortais, *Angew. Chem., Int. Ed.*, 2019, **58**, 6727–6731; (*f*) Y. Su, D. Zhu, Z. Ma, Y. Wang, Z. Wang, Z. Wang, Y. Ma and W.-H. Sun, *RSC Adv.*, 2025, **15**, 23097–23102; (*g*) Z. Wang, N. Ma, X. Lu, M. Liu, T. Liu, Q. Liu, G. A. Solan and W.-H. Sun, *Dalton Trans.*, 2023, **52**, 10574–10583.
11 A. Dubey, S. M. W. Rahaman, R. R. Fayzullin and J. R. Khusnutdinova, *ChemCatChem*, 2019, **11**, 3844–3852.
12 A. Dubey, L. Nencini, R. R. Fayzullin, C. Nervi and J. R. Khusnutdinova, *ACS Catal.*, 2017, **7**, 3864–3868.
13 A. Srinivasan, J. Campos, N. Giraud, M. Robert and O. Rivada-Wheelaghan, *Dalton Trans.*, 2020, **49**, 16623–16626.
14 K. Patra, R. A. Laskar, A. Nath and J. K. Bera, *Organometallics*, 2022, **41**, 1836–1846.
15 K. Patra, A. Bhattacherya, C. Li, J. K. Bera and H. S. Soo, *ACS Catal.*, 2022, **12**, 15168–15180.
16 K. Bera and A. Mukherjee, *Chem. – Asian. J.*, 2023, **18**, e202300157.
17 C. Zhang, B. Hu, D. Chen and H. Xia, *Organometallics*, 2019, **38**, 3218–3226.
18 H.-J. Pan, G. Huang, M. D. Wodrich, F. F. Tirani, K. Ataka, S. Shima and X. Hu, *Nat. Chem.*, 2019, **11**, 669–675.
19 G.-W. Wang, M.-W. Chen, Y.-Q. Wu, Q.-X. Xie, Z. Liu, R.-Z. Liao and Y.-G. Zhou, *ACS Catal.*, 2025, **15**, 3418–3427.
20 S. Nandi, I. Borthakur, K. Ganguli and S. Kundu, *Organometallics*, 2023, **42**, 1793–1802.
21 R. Van Putten, J. Benschop, V. J. De Munck, M. Weber, C. Müller, G. A. Filonenko and E. A. Pidko, *ChemCatChem*, 2019, **11**, 5232–5235.
22 K. Patra, R. A. Laskar, A. Nath and J. K. Bera, *Organometallics*, 2022, **41**, 1836–1846.
23 J. Yang, Y. Guo, Z. Wang, Y. Wang, D. Fu, Q. Liu, G. A. Solan, Y. Ma and W.-H. Sun, *Org. Lett.*, 2025, **27**, 2564–2568.

24 Z. Wang, S. Zhang, Z. Ma, L. Li, X. Yan, Q. Cao, Y. Su, N. Ma and Z. Wang, *Mol. Catal.*, 2024, **564**, 114274.
25 Y. Xu, Z. Zhang, Y. Wang, L. Li, N. Ma, Z. Wang, H. Li, Y. Ma and W.-H. Sun, *J. Catal.*, 2026, **456**, 116732.
26 Y. Su, D. Zhu, Z. Ma, Y. Wang, Z. Wang, Z. Wang, Y. Ma and W.-H. Sun, *RSC Adv.*, 2025, **15**, 23097–23102.
27 K. Ganguli, S. Shee, D. Panja and S. Kundu, *Dalton Trans.*, 2019, **48**, 7358–7366.
28 J. Yang, L. Yao, Z. Wang, Z. Zuo, S. Liu, P. Gao, M. Han, Q. Liu, G. A. Solan and W.-H. Sun, *J. Catal.*, 2023, **418**, 40–50.
29 A. Zirakzadeh, S. R. M. M. de Aguiar, B. Stöger, M. Widhalm and K. Kirchner, *ChemCatChem*, 2017, **9**, 1744–1748.
30 C. Liu, R. van Putten, P. O. Kulyaev, G. A. Filonenko and E. A. Pidko, *J. Catal.*, 2018, **363**, 136–143.
31 P. A. Dub and J. C. Gordon, *ACS Catal.*, 2017, **7**, 6635–6655.
32 H. Jayaprakash, P. Coburger, M. Wörle, A. Togni and H. Grützmacher, *Chem. – Eur. J.*, 2022, **28**, e202201522.
33 M. Garbe, K. Junge, S. Walker, Z. Wei, H. Jiao, A. Spannenberg, S. Bachmann, M. Scalone and M. Beller, *Angew. Chem., Int. Ed.*, 2017, **56**, 11237–11241.
34 S. J. P. Spall, T. Keane, J. Tory, D. C. Cocker, H. Adams, H. Fowler, A. J. H. M. Meijer, F. Hartl and J. A. Weinstein, *Inorg. Chem.*, 2016, **55**, 12568–12582.
35 H. Liu, S.-B. Ko, H. Josien and D. P. Curran, *Tetrahedron Lett.*, 1995, **36**, 8917–8920.
36 R. A. Coburn and G. O. Dudek, *J. Phys. Chem.*, 1968, **72**, 1177–1181.
37 C. M. Alvarez, R. García-Rodríguez and D. Miguel, *Dalton Trans.*, 2007, 3546–3554.
38 Z. Wang, L. Chen, G. Mao and C. Wang, *Chin. Chem. Lett.*, 2020, **31**, 1890–1894.
39 Z. Wang, N. Ma, X. Lu, M. Liu, T. Liu, Q. Liu, G. A. Solan and W.-H. Sun, *Dalton Trans.*, 2023, **52**, 10574–10583.
40 Z. Wang, Q. Lin, N. Ma, S. Liu, M. Han, X. Yan, Q. Liu, G. A. Solan and W.-H. Sun, *Catal. Sci. Technol.*, 2021, **11**, 8026–8036.
41 O. Martínez-Ferraté, C. Werlé, G. Franciò and W. Leitner, *ChemCatChem*, 2018, **10**, 4514–4518.
42 N. F. Both, J. Fessler, A. Vicenzi, K. Andres, A. Spannenberg, K. Junge and M. Beller, *ChemCatChem*, 2024, **16**, e202301562.
43 L. Falivene, Z. Cao, A. Petta, L. Serra, A. Poater, R. Oliva, V. Scarano and L. Cavallo, *Nat. Chem.*, 2019, **11**, 872–879.
44 K. Dey and G. de Ruiter, *Org. Lett.*, 2024, **26**, 4173–4177.
45 D. P. Zobernig, M. Luxner, B. Stöger, L. F. Veiros and K. Kirchner, *Chem. – Eur. J.*, 2024, **30**, e202302455.
46 C. L. Oates, A. S. Goodfellow, M. Bühl and M. L. Clarke, *Angew. Chem., Int. Ed.*, 2023, **62**, e202212479.
47 A. S. Goodfellow, M. L. Clarke and M. Bühl, *Chem. – Eur. J.*, 2025, **31**, e202501063.
48 A. M. Krieger, V. Sinha, G. Li and E. A. Pidko, *Organometallics*, 2022, **41**(14), 1829–1835.
49 A. Kundu, B. Mandal, B. Maji and D. Adhikari, *J. Phys. Chem. A*, 2023, **127**(48), 10068–10074.
50 T. Nguyen, M. A. Wicki and V. Snieckus, *J. Org. Chem.*, 2004, **69**, 7816–7821.
51 B. Abarca, F. Mojarred, G. Jones, C. Phillips, N. Ng and J. Wastling, *Tetrahedron*, 1988, **44**, 3005–3014.
52 S. T. Goralski, T. A. Manes, S. E. A. Lumsden, V. M. Lynch and M. J. Rose, *Organometallics*, 2020, **39**, 1070–1079.
53 D. Peng, Y. Zhang, X. Du, L. Zhang, X. Leng, M. D. Walter and Z. Huang, *J. Am. Chem. Soc.*, 2013, **135**, 19154–19166.
54 S. Grimme, J. Antony, S. Ehrlich and H. Krieg, *J. Chem. Phys.*, 2010, **132**, 154104.
55 P. J. Stephens, F. J. Devlin, C. F. Chabalowski and M. J. Frisch, *J. Phys. Chem.*, 1994, **98**, 11623–11627.
56 F. Neese, F. Wennmohs, U. Becker and C. Riplinger, *J. Chem. Phys.*, 2020, **152**, 224108.
57 F. Neese, *Wiley Interdiscip. Rev. Comput. Mol. Sci.*, 2022, **12**, e1606.
58 F. Weigend and R. Ahlrichs, *Phys. Chem. Chem. Phys.*, 2005, **7**, 3297–3305.
59 F. Weigend, *Phys. Chem. Chem. Phys.*, 2006, **8**, 1057–1065.
60 L. A. Curtiss, M. P. McGrath, J. Blaudeau, N. E. Davis, R. C. Binning Jr and L. Radom, *J. Chem. Phys.*, 1995, **103**, 6104–6113.
61 M. J. Frisch, J. A. Pople and J. S. Binkley, *J. Chem. Phys.*, 1984, **80**, 3265–3269.
62 T. Clark, J. Chandrasekhar, G. W. Spitznagel and P. V. R. Schleyer, *J. Comput. Chem.*, 1983, **4**, 294–301.
63 W. J. Hehre, R. Ditchfield and J. A. Pople, *J. Chem. Phys.*, 1972, **56**, 2257–2261.
64 A. V. Marenich, C. J. Cramer and D. G. Truhlar, *J. Phys. Chem. B*, 2009, **113**, 6378–6396.
65 C. Y. Legault, *CYLview20*, Université de Sherbrooke, 2020.
66 (*a*) CCDC 2540706: Experimental Crystal Structure Determination, 2026, DOI: 10.5517/ccdc.csd.cc2r8t84; (*b*) CCDC 2540707: Experimental Crystal Structure Determination, 2026, DOI: 10.5517/ccdc.csd.cc2r8t95; (*c*) CCDC 2540708: Experimental Crystal Structure Determination, 2026, DOI: 10.5517/ccdc.csd.cc2r8tb6; (*d*) CCDC 2540709: Experimental Crystal Structure Determination, 2026, DOI: 10.5517/ccdc.csd.cc2r8tc7; (*e*) CCDC 2540710: Experimental Crystal Structure Determination, 2026, DOI: 10.5517/ccdc.csd.cc2r8td8; (*f*) CCDC 2540711: Experimental Crystal Structure Determination, 2026, DOI: 10.5517/ccdc.csd.cc2r8tf9; (*g*) CCDC 2540712: Experimental Crystal Structure Determination, 2026, DOI: 10.5517/ccdc.csd.cc2r8tgb; (*h*) CCDC 2540713: Experimental Crystal Structure Determination, 2026, DOI: 10.5517/ccdc.csd.cc2r8thc; (*i*) CCDC 2540714: Experimental Crystal Structure Determination, 2026, DOI: 10.5517/ccdc.csd.cc2r8tjd; (*j*) CCDC 2540715: Experimental Crystal Structure Determination, 2026, DOI: 10.5517/ccdc.csd.cc2r8tkf.